A Transmission-Dependent Method for Scatter Correction in SPECT

Steven R. Meikle, Brian F. Hutton and Dale L. Bailey

Department of Nuclear Medicine, Royal Prince Alfred Hospital, Sydney, Australia

A method of scatter compensation has been developed that incorporates planar transmission measurements in the estimation of photopeak scatter in SPECT. **Methods:** The scatter distribution is first estimated by convolving the planar projections with a monoexponential scatter function. The number of scattered events that subsequently reach the detector as a proportion of total events (i.e., scatter fraction) is then determined for each point in the projections based on narrow-beam transmission values, obtained using an external source. The assumptions of the method were tested using ^{99m}Tc and ^{201}Tl point and line sources. The quantitative and qualitative impact of transmission-dependent scatter correction was assessed in realistic phantom experiments simulating blood-pool, lung and myocardial perfusion studies. **Results:** The method accurately predicts the scatter distribution from ^{99m}Tc and ^{201}Tl line sources in a phantom with variable density. Reconstructed counts are artificially enhanced in regions of high tissue density when scattered events are not removed from the projections prior to attenuation correction. Using convolution-subtraction with a constant scatter fraction (k = 0.4), scatter is underestimated in the heart and overestimated in the lungs, whereas transmission-dependent scatter correction enables activity to be quantified with ≥95% accuracy in heart and lung regions. **Conclusion:** We conclude that incorporating transmission data enables accurate scatter compensation in objects with nonuniform density.

Key Words: Compton scattering; transmission tomography; attenuation correction; quantitative SPECT

J Nucl Med 1994; 35:360–367

Attenuation and Compton scattering of emitted photons are the main factors that limit the quantitative accuracy of single-photon emission computed tomography (SPECT). Although no analytically exact solution to the attenuation problem has been found, sufficient accuracy can be achieved using transmission measurements (*1,2*), particularly when combined with iterative correction techniques (*3–7*). Various scatter compensation methods have also been described (*8–16*) but few have addressed the complex scattering problem in objects with heterogeneous density such as the thorax.

In order for a scatter correction method to be useful clinically, it should be applicable for a range of radionuclides, most importantly ^{99m}Tc and ^{201}Tl, and it should be able to accurately estimate scatter in a heterogeneous object. The most commonly employed methods, because of their practicality, are the convolution-subtraction (*8*) and lower energy window subtraction methods (*9*). The convolution-subtraction method makes simplifying assumptions that do not hold when the scattering medium is heterogeneous (*17*), particularly the assumption of a constant scatter fraction (the ratio of scattered-to-total events). Although the lower energy window method inherently accounts for object heterogeneity, quantitative accuracy is inferior to deconvolution approaches and the appropriate value by which to scale the lower window scatter image is object- and instrumentation-dependent (*18*). Although the method has been successfully applied to ^{201}Tl imaging (*19*), the assumption that scattered events recorded in the two energy windows are equivalent has not been tested for such low energy sources (main emissions 68–83 keV). Methods based on information obtained from energy spectra acquired at different spatial locations (*11,13*) may be more suitable for ^{201}Tl. However, these approaches require specialized hardware to allow acquisition of many energy spectra and, consequently, have not been widely used.

More recently, a scatter correction method has been introduced that uses position-dependent scatter functions derived a priori by Monte Carlo simulations (*14*). This method takes into account the spatial variation in scatter and has been tested in objects with nonuniform density (*20*). However, the correction is based on one-dimensional scatter line spread functions and, therefore, does not take into account out-of-plane scattering. Furthermore, because of the need to perform several Monte Carlo experiments for each new imaging geometry and radionuclide, this method may not be practical. A method that uses a split window over the ^{99m}Tc photopeak shows promise for practical and accurate scatter correction (*16*). With significant modification, the split window approach has been applied to ^{111}In imaging (*21*) and can, in principle, be extended for use with ^{201}Tl sources. However, this validation has not yet been performed.

We have previously investigated the feasibility of using

Received Mar. 18, 1993; revision accepted Nov. 5, 1993.

For correspondence or reprints contact: Steven Meikle, Department of Nuclear Medicine, Royal Prince Alfred Hospital, Missenden Road, Camperdown, NSW 2050, Australia.

transmission data to improve the accuracy of scatter correction in the presence of nonuniform density (*17,22*). In this paper, the assumptions of the transmission-based scatter model have been tested and the method validated for use with ^{99m}Tc and ^{201}Tl sources. The accuracy of the method has been assessed in phantom and human studies representing a range of clinical applications including blood pool, lung and myocardial perfusion studies. We have concentrated on studies of the thorax as these pose the most challenging geometries for quantitative SPECT. However, the results can also be applied to other imaging situations.

MATERIALS AND METHODS

Theory

The scatter correction method we propose is applied to two-dimensional planar projections obtained during a SPECT acquisition. It is based on the convolution-subtraction method (*8*) which assumes that the scatter response function is spatially invariant and that the scatter fraction is constant throughout the object being imaged. Using the geometric mean of opposing projections, we have previously shown that the slope of the scatter function is reasonably independent of attenuation. However, scatter fraction varies with both object density and size (*17*). Therefore, the distribution of scattered events, g_{sc}, is initially estimated by convolving the measured photopeak projection, g_{obs} (after calculating the geometric mean), with a radially symmetric monoexponential scatter function, s:

$$g_{sc} = g_{obs} \otimes s, \qquad \text{Eq. 1}$$

where $\otimes$ denotes two-dimensional convolution. Using Axelsson's approach (*8*), the scatter estimate is scaled by a constant scatter fraction, determined experimentally. Our approach differs in that scatter fraction is treated as a variable which is calculated at each point in the two-dimensional matrix.

First, let us consider a point source measured at depth, d, in an attenuating material. The scatter fraction, k, can be written in terms of broad-beam (including scatter) and narrow-beam (excluding scatter) counts as:

$$k = \frac{C_{broad} - C_{narrow}}{C_{broad}} = 1 - \frac{1}{B(d)}, \qquad \text{Eq. 2}$$

where B is the depth-dependent buildup factor which, by definition (*23*), is the ratio of broad-beam-to-narrow-beam counts at depth d in the object. Wu et al. (*24*) derived a buildup function of the form $A - Be^{-md}$, where A, B and m are constants experimentally determined. We have shown previously that a more generalized equation is given by $A - Be^{-\beta\mu d}$ which describes the buildup for a given attenuation path length, μd (*17*). By substituting the modified buildup equation into Equation 2, we obtain:

$$k = 1 - \frac{1}{A - Be^{-\beta\mu d}}. \qquad \text{Eq. 3}$$

If the point source is measured from conjugate views and the geometric mean of those views is calculated, the point-spread function including scatter (and, therefore, scatter fraction) is approximately equivalent to that from a source at the center of the object, independent of depth (*25*). Therefore, Equation 3 can be rewritten as:

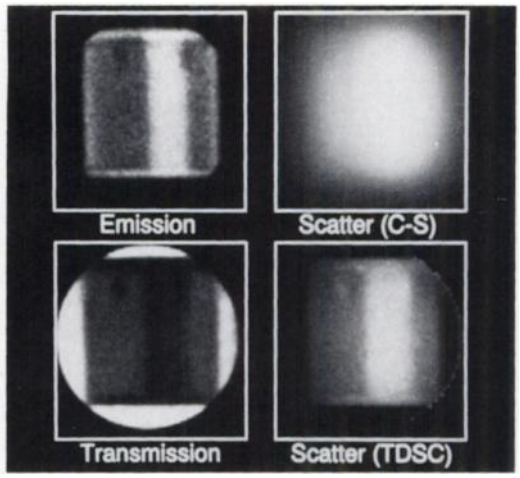

FIGURE 1. Planar images of a thorax phantom illustrating the differences between convolution-subtraction (C-S) and transmission-dependent scatter correction (TDSC). The top row shows the emission distribution and the scatter estimate using the C-S method. The bottom row shows the planar transmission scan and the corresponding scatter estimate using TDSC. TDSC predicts zero scatter outside the body where attenuation is negligible.

$$k = 1 - \frac{1}{A - Be^{-\beta\mu T/2}} = 1 - \frac{1}{A - B(e^{-\mu T})^{\beta/2}}, \qquad \text{Eq. 4}$$

where T is the total object thickness. The exponential term in Equation 4 is equivalent to the ratio of attenuated-to-unattenuated counts for an external source, or transmission factor. Thus, we now have an equation that relates scatter fraction to narrow-beam transmission factor, with A, B and beta constants to be determined. In practice, transmission factors can be determined for every point in the projection by dividing a planar transmission scan (using a flood source for example) by a blank scan (performed without the object in the field of view). From this, a two-dimensional matrix of scatter fractions, K, can be calculated:

$$K(x, y) = 1 - \frac{1}{A - Bt(x, y)^{\beta/2}}, \qquad \text{Eq. 5}$$

where t(x, y) is the narrow-beam transmission factor measured at (x, y). The scatter estimate obtained by Equation 1 is scaled by the two-dimensional matrix of scatter fractions calculated above and subtracted from the photopeak projection.

The constant B can be substituted with (A − 1) if we wish to constrain the scatter fraction to zero at zero depth or zero attenuation. In this case, the transmission-based model predicts zero scatter outside the body where attenuation is negligible, and the scatter estimate differs noticeably from that obtained by conventional convolution-subtraction (*8*) as illustrated in Figure 1. The process can be repeated iteratively (*22*) using the current scatter-free estimate, g_{n-1}, as the subject of the convolution to determine an updated estimate, g_n:

$$g_n = g_{obs} - K(g_{n-1} \otimes s). \qquad \text{Eq. 6}$$

With each iteration, the function g_{n-1} approaches the scatter-free projection we are trying to estimate. Therefore, this approach complies better with the convolution model since the scatter function, s, is, by definition, the response to a "scatter-free" source when placed in a scattering medium. However, the effect of the

number of iterations was not the subject of this investigation. Therefore, all results reported are for a single iteration of transmission-dependent scatter correction.

Scatter Fraction Versus Narrow-Beam Transmission

Point sources of ^{99m}Tc and ^{201}Tl were counted separately in varying depths of water (0–16 cm) keeping source-to-detector distance constant. These and all subsequent measurements were made on a large field of view (LFOV) gamma camera (Philips DiagnosTomo, Hamburg, Germany) with a low-energy general purpose (LEGP) collimator. A 20% symmetric window was used for both radionuclides and only the low energy (74 keV, 88%) emissions of ^{201}Tl were recorded. The decay-corrected counts for the entire field of view represent broad-beam measurements as photopeak scatter is included. Corresponding narrow-beam values at each depth were calculated by applying published narrow-beam attenuation coefficients for ^{99m}Tc and ^{201}Tl (*26*) to the measurements made in air. Scatter fractions were calculated from these measurements using Equation 2. These were plotted against narrow-beam transmission factors for two transmission sources, ^{99m}Tc and ^{153}Gd, and fitted using nonlinear least squares to determine the parameters of Equation 4.

Validation by Line Source Measurements

A line source containing approximately 100 MBq of ^{99m}Tc was positioned in the center of an elliptical water-filled cylinder (axes 28.5 cm × 20 cm, length 30 cm) next to a 10-cm diameter cylinder containing only air. This configuration was imaged in the anterior and posterior projections from which a geometric mean projection was calculated. A transmission scan was also performed using a collimated ^{153}Gd line source. This experiment was repeated using a ^{201}Tl line source containing approximately 30 MBq. In each case, scatter was estimated by the convolution-subtraction method using a scatter fraction of 0.4 for ^{99m}Tc and 0.5 for ^{201}Tl (based on results of the scatter fraction experiment) and by the transmission-dependent method. The slope of the monoexponential scatter function was 0.24 cm^{-1} for ^{99m}Tc and 0.19 cm^{-1} for ^{201}Tl. Accuracy was assessed by the fit of the scatter estimates to the measured scatter tails using logarithmic count profiles.

Phantom Studies

Three experiments were performed using a realistic thorax phantom to assess the quantitative and qualitative effect of transmission-dependent scatter correction in a range of clinical imaging situations. The phantom is elliptical (axes 30 cm × 20 cm, length 30 cm) and contains lung-shaped cylinders filled with polystyrene beads suspended in water, providing density similar to lung tissue as well as a perspex section placed posteriorly simulating the spine. In the first experiment, the cardiac and background sections were filled with water containing 0.0325 MBq · ml^{-1} of ^{99m}Tc simulating a blood-pool study. In the second experiment, a lung perfusion study was simulated by adding 195 MBq of ^{99m}Tc to the lungs with no activity in the cardiac or background sections. In the third experiment, an annular myocardial insert containing 0.014 MBq · ml^{-1} of ^{201}Tl was placed in the cardiac section while the lungs and background sections contained 0.0035 MBq · ml^{-1} of ^{201}Tl. These activities were chosen to give approximately a 4:1 ratio between myocardium and background simulating a ^{201}Tl myocardial perfusion study. SPECT acquisitions were performed using 360° rotation, 64 projection angles and 20 sec per angle for the ^{99m}Tc studies, 30 sec per angle for the ^{201}Tl study. Transmission data were acquired using a scanning collimated line source (*27*) containing ^{99m}Tc for the ^{99m}Tc studies and ^{153}Gd for the ^{201}Tl study. Prior to reconstruction, the projections were prefiltered using a two-dimensional fourth-order Butterworth filter. The cut-off frequency, v_c, was equal to half the Nyquist frequency (Nyq) for the ^{99m}Tc studies and 0.3 Nyq for the ^{201}Tl study.

Quantitative accuracy was assessed in the blood-pool and lung experiments using four correction schemes that vary in ease of implementation and the number of assumptions made about the imaging process. The first method ignored scatter and used the first step of the Chang attenuation correction procedure (*28*), assuming an elliptical body outline and a constant broad-beam attenuation coefficient of 0.08 cm^{-1}, which is an average for lung and soft-tissue regions. This approach is common for obtaining approximate quantification and the software is widely available on commercial SPECT systems. In the second approach, the same attenuation correction method was applied; however, the projections were first scatter-corrected using the convolution-subtraction method (*8*) (slope = 0.24 cm^{-1}, k = 0.4) and a narrow-beam average μ value, 0.1 cm^{-1}, was used. This scatter correction method is less widely available but is straightforward to implement. The remaining two methods require transmission measurements.

In method three, convolution-subtraction was again used to correct for scatter, but attenuation correction was performed using a two-step procedure incorporating the measured attenuation data (*29*). Briefly, the first step involves a postreconstruction multiplicative correction as in Chang's noniterative procedure (*28*), except that the reconstructed attenuation map is used instead of a simple body outline and constant attenuation coefficient. This is followed by a forward projection step in which the measured projections are modified, based on the ratio of projections with and without the inclusion of attenuation (*30,31*), and then reconstructed. Finally, transmission-dependent scatter correction using planar transmission data was applied in conjunction with the two-step attenuation correction procedure. The scatter and attenuation corrections used in this scheme make no assumptions about the geometry or attenuation of the object.

Quantitative accuracy, using the methods described above, was calculated for the blood-pool and lung studies by comparing reconstructed activity (or activity concentration) with the calibrated amount. Camera efficiency was measured using a 6-cm diameter source in a shallow dish placed 8 cm from the collimator face. Along with the quantitative comparison, the qualitative impact of scatter correction was assessed in all three experiments by comparing reconstructed images with and without scatter correction. For the qualitative comparison, only the latter two methods were employed. When scatter correction was not applied, attenuation maps were scaled to broad-beam values to account for the inclusion of scatter in the measurement.

Human Study

A 46-yr-old female undergoing a routine ^{201}Tl myocardial perfusion study was administered 120 MBq of ^{201}Tl-chloride at maximal exercise. In addition to routine imaging, a simultaneous emission-transmission study was performed immediately following the postexercise study, using ^{153}Gd as the transmission source (*27*). Sixty-four projection angles were acquired over 360° at 40 sec per angle. The projections were prefiltered using a fourth-order Butterworth filter with v_c = 0.3 Nyquist and reconstructed using three methods: (1) no scatter or attenuation correction, (2) attenuation correction only and (3) transmission-dependent scatter correction and attenuation correction. Attenuation correction was performed as a two-step procedure as in Method 4 of the phantom studies.

TABLE 1
Fitted Parameter Values for Scatter Fraction Determination Using Various Emission and Transmission Radionuclides

Emission radionuclide	Transmission radionuclide	A	B	Beta	r*
^{99m}Tc	^{99m}Tc	3.6 ± 0.9	2.6 ± 0.9	0.15 ± 0.05	0.998
^{99m}Tc	^{153}Gd	3.6 ± 0.9	2.6 ± 0.8	0.13 ± 0.05	0.998
^{201}Tl	^{99m}Tc	3.7 ± 0.5	2.7 ± 0.5	0.26 ± 0.06	0.997
^{201}Tl	^{153}Gd	3.7 ± 0.5	2.7 ± 0.5	0.23 ± 0.05	0.998

*Correlation coefficient for the regression between measured and estimated scatter fraction using narrow-beam transmission factors and the fitted parameters.

Attenuation maps were scaled to broad-beam values for the second case where no scatter correction was applied. The transaxial images were reoriented into 8 mm thick short-axis slices for comparison using identical reslice parameters.

RESULTS

Scatter Fraction versus Narrow-beam Transmission

The correlation between measured scatter fractions and those predicted from narrow-beam transmission measurements was excellent ($r > 0.99$) for each radionuclide combination. Fitted values for the constants in Equation 4 are shown in Table 1. Only parameter beta appears to depend significantly on photon energy with very little variation in the values of A and B for the various radionuclide combinations. The value of B was in all cases approximately equal to A − 1, supporting the assumption of zero scatter fraction at zero depth or attenuation. Figure 2 shows ^{99m}Tc and ^{201}Tl scatter fractions plotted against transmission factor using ^{153}Gd as the transmission radionuclide. The graph shows that most of the variation in scatter fraction (0%–33% for ^{99m}Tc and 0%–45% for ^{201}Tl) occurs between transmission factors of 1 and 5 corresponding to depths of 0–10 cm in water. At depths greater than 10 cm, scatter fraction plateaus at about 0.4 for ^{99m}Tc and 0.5 for ^{201}Tl. This was the basis for using these values when applying the convolution-subtraction method in phantom and human studies.

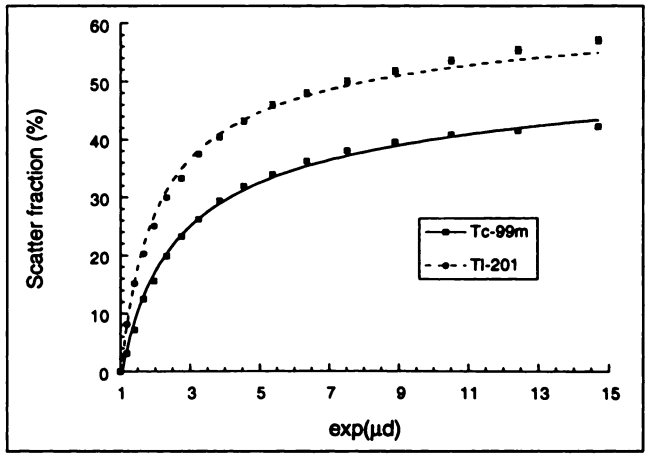

FIGURE 2. Measured scatter fractions for ^{99m}Tc and ^{201}Tl point sources in water versus narrow-beam transmission factor using a ^{153}Gd transmission source. The solid and dashed lines are the fitted curves for ^{99m}Tc and ^{201}Tl, respectively, using the modified buildup equation.

Validation By Line Source Measurements

Scatter estimates obtained by convolution-subtraction and the transmission-dependent method are shown as logarithmic plots in Figure 3. The scatter tails are clearly asymmetric in both the ^{99m}Tc and ^{201}Tl plots due to the presence of the air cylinder. Convolution-subtraction estimates a much broader distribution than the true scatter and does not correctly predict asymmetry. As a result, scatter is underestimated near the source and overestimated further away from the source. The transmission-dependent method gives a good fit to the scatter tails for both the ^{99m}Tc and ^{201}Tl sources and correctly predicts an asymmetric point scatter distribution due to variable attenuation.

Phantom Studies

Results of the activity quantification experiments are shown in Table 2. Using method 1, where no scatter correction was performed and a simple attenuation correction was used, accuracy is good in the heart but very poor in the lungs. Accuracy is improved in the lungs by employing scatter correction using convolution-subtraction, but at the expense of accuracy in the heart. Using convolution-subtraction in combination with accurate attenuation correction incorporating measured attenuation data, quantitative errors are less than 10% in both studies. However, there is still an appreciable overestimation of activity in the heart and underestimation of activity in the lungs, the relative error being almost 20%. Accuracy is further improved using transmission-dependent scatter correction in combination with the two-step attenuation correction, resulting in quantitative errors that are ≤5% in both the heart and lung regions and a relative error of <10%.

Figure 4 shows the effect of scatter correction on objects with heterogeneous density such as the thorax. In all three experiments, artifacts were observed when attenuation correction was applied without first performing scatter compensation. The artifacts manifest as increased counts in high density regions including the heart and spine as indicated by the arrows. The artifacts were removed and contrast improved by performing scatter correction prior to attenuation correction, using both convolution-subtraction and transmission-dependent scatter correction. However, the quantitative results suggest that the improvement in contrast using convolution-subtraction may be due in part to oversubtraction of scatter in the lung regions. This was confirmed by count profiles through the heart and lungs of the reconstructed blood-pool image shown in Figure 5. The profiles demonstrate significant negative values in the region of the lungs using convolution-subtraction, whereas transmission-dependent scatter correction correctly predicts zero activity concentration.

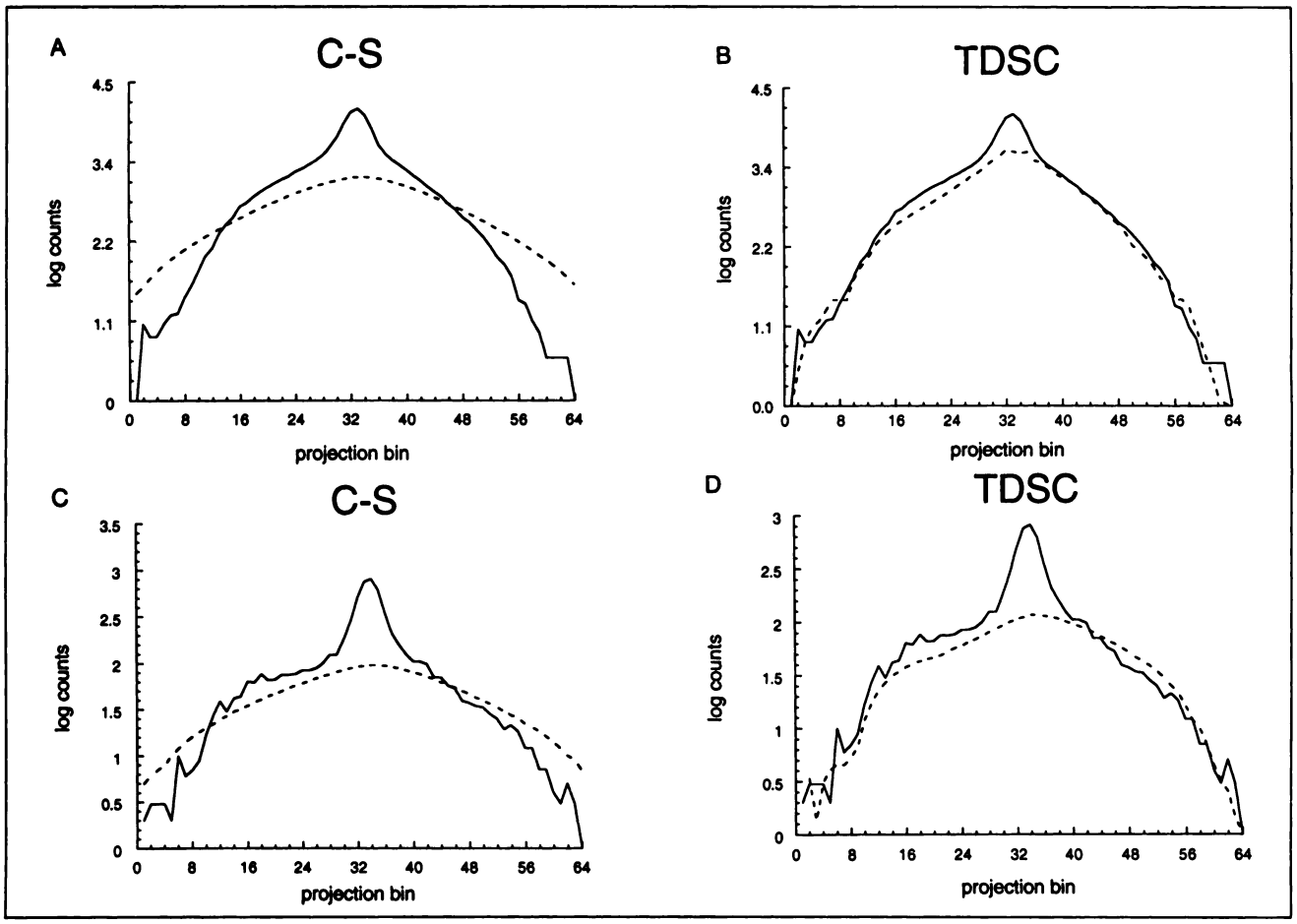

FIGURE 3. Logarithmic count profiles, indicated by the solid curves, of a ^{99m}Tc (A and B) and a ^{201}Tl (C and D) line source adjacent to an air cylinder in an elliptical water-filled phantom. The dashed curves are the scatter estimates using the convolution-subtraction (C-S) method with a scatter fraction of 0.4 for ^{99m}Tc and 0.5 for ^{201}Tl and transmission-dependent scatter correction (TDSC).

Human Study

A midventricular short-axis slice is shown in Figure 6 for each of the three processing methods applied. The image on the left was reconstructed without correction for scatter or attenuation. The middle image was reconstructed with attenuation correction only, and the image on the right was reconstructed with transmission-dependent scatter and attenuation correction. Shown underneath each image are the corresponding count profiles through the myocardium along the line indicated. Without attenuation correction, the counts in the infero-septal wall are appreciably reduced relative to the rest of the myocardium. This attenuation

TABLE 2
Activity Quantification in Blood-Pool and Lung Phantom Studies

Method*	Blood-pool study (calibrated conc. = 0.0325 MBq · ml^{-1})		Lung perfusion study (calibrated activity = 195 MBq)	
	Measured	Error (%)	Measured	Error (%)
No SC + Chang	0.0340	+5	264	+35
C-S + Chang	0.0300	−8	216	+11
C-S + two-step AC	0.0354	+9	178	−9
TDSC + two-step AC	0.0342	+5	188	−4

*Four quantitative correction methods were employed, including: (1) No scatter correction (No SC) plus Chang multiplicative attenuation correction (AC) using an average broad-beam μ value; (2) convolution-subtraction (C-S) plus Chang AC using an average narrow-beam μ value; (3) C-S plus two-step AC using measured attenuation data; (4) transmission-dependent scatter correction (TDSC) plus two-step AC using measured attenuation data.

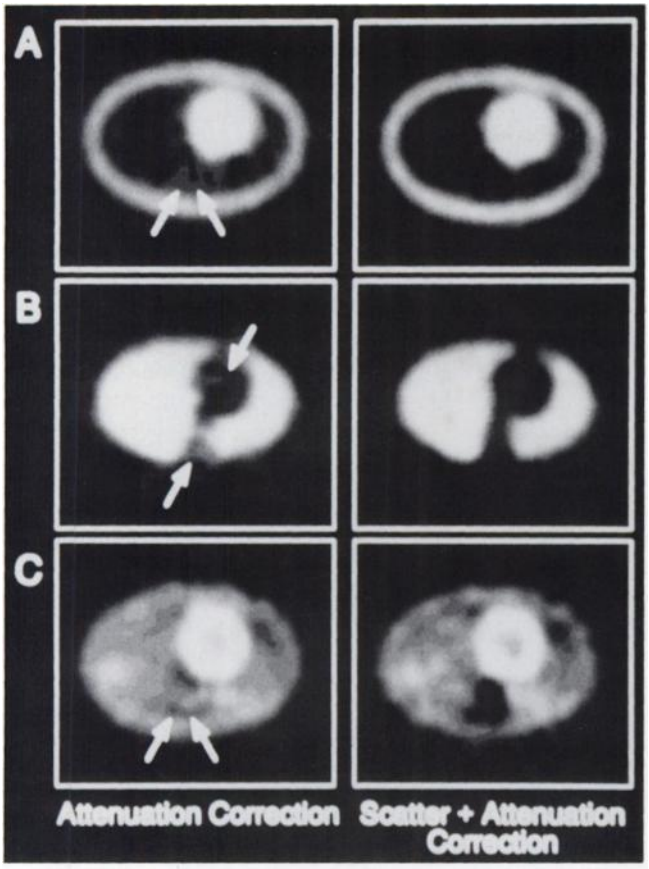

FIGURE 4. Reconstructed images of the thorax phantom used to simulate (A) a ^{99m}Tc blood-pool study; (B) a ^{99m}Tc lung perfusion study and (C) a ^{201}Tl myocardial perfusion study. Attenuation correction was applied as a two-step procedure incorporating measured attenuation data (see text). The images on the right were also processed using transmission-dependent scatter correction prior to attenuation correction. In each experiment, counts in high density regions such as the heart and spine were artificially enhanced (indicated by arrows) when scatter correction was not performed prior to attenuation correction.

artifact is typical in myocardial perfusion studies (*7*) and is removed by accurate attenuation correction. By performing both scatter and attenuation correction, myocardial activity is more uniform and image contrast is improved, as indicated by the count profiles.

DISCUSSION

The results shown in Table 2 demonstrate that, in general, accurate quantification cannot be achieved when assumptions about object density and geometry are made in either the scatter or attenuation correction procedures. Using the first two methods, where the assumption of constant attenuation is made, the effective μ value can be tailored to achieve good accuracy in either the heart or lung. However, one cannot achieve accuracy throughout a heterogeneous object using these methods. Similarly, using convolution-subtraction in combination with accurate attenuation correction, as in Method 3, the constant scatter fraction can be tailored to achieve good accuracy in the

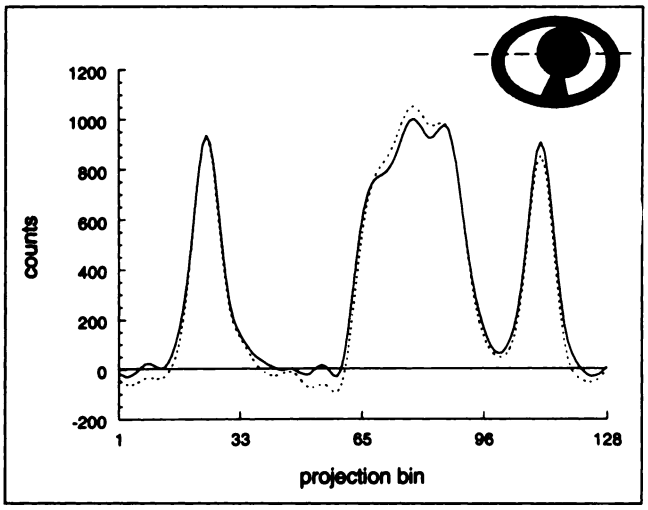

FIGURE 5. Horizontal count profiles through the reconstructed images of the ^{99m}Tc blood-pool phantom using convolution-subtraction with a scatter fraction of 0.4 (dashed line) and transmission-dependent scatter correction (solid line). Note the negative values in the lung using the convolution-subtraction method, resulting from oversubtraction of scatter.

heart, for example, but at the expense of accuracy in the lungs. In our study, using a scatter fraction of 0.4, activity in the organ of interest was overestimated in the blood-pool study and underestimated in the lung study. Therefore, a scatter fraction of 0.4 is too low for high density regions such as the heart and too high for low density regions such as the lungs. These results, and the graphs of scatter frac-

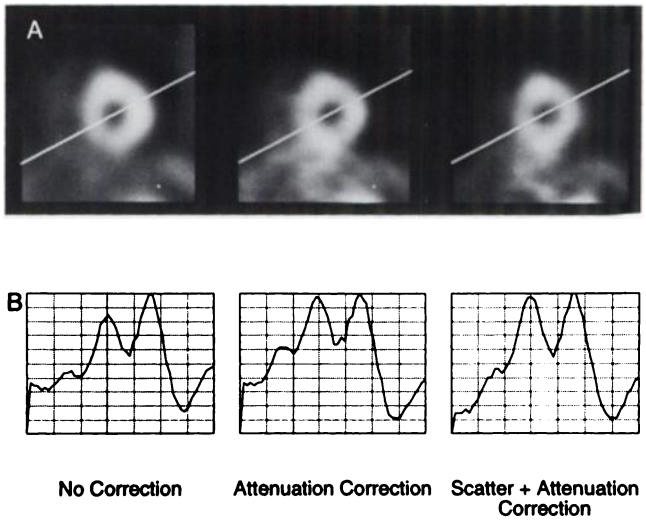

FIGURE 6. (A) Short-axis reconstructions of a clinical ^{201}Tl myocardial perfusion study and (B) corresponding count profiles along the line indicated through the myocardium. The images were processed using no scatter or attenuation correction (left), attenuation correction only (middle) and scatter correction followed by attenuation correction (right). Both scatter and attenuation correction methods incorporated transmission data that were acquired simultaneously with the emission data using a scanning collimated line source.

tion versus transmission factor shown in Figure 2, suggest that it is inappropriate to use a constant scatter fraction when the object has nonuniform density. The use of a constant scatter fraction may result in negative reconstructed values, as well as reducing quantitative accuracy, resulting in artificially high contrast (Fig. 5).

The improvement in accuracy of scatter estimation by taking into account variable attenuation was demonstrated by the line source measurements and by the results of the activity quantification experiments. Using transmission-dependent scatter correction with measured attenuation correction, quantitative estimates were within 5% of the calibrated values. This was achieved in two separate imaging examples, in which the organ of interest had quite different attenuating properties, demonstrating that accuracy in SPECT reconstructions throughout the object is possible with the transmission-based approach. Although convolution-subtraction, when used in conjunction with measured attenuation correction, also achieved good quantitative accuracy, the relative error between lung and blood-pool measurements was almost 20%, compared with <10% using the transmission-based approach. This accuracy may be sufficient for many clinical applications, including myocardial perfusion imaging. However, in other examples, such as tumor quantification studies, the ability to accurately determine activity independent of location in the body and attenuation of the surrounding tissue, is clearly desirable.

Variable attenuation has previously been shown to introduce artifacts due to enhanced transmission through areas of low attenuation (*6*). This causes artificially increased reconstructed counts in low density regions such as the lungs. In simulations, which allow the effect of attenuation alone to be studied, iterative compensation combined with measured attenuation data removes the inconsistencies and eliminates artifacts. However, the images in Figure 4 demonstrate that accurate attenuation correction alone does not remove all artifacts when scattered events are also present in the measured data. Indeed, by removal of attenuation artifacts, the remaining artifacts, which are due to scatter, are more apparent. They manifest as increased reconstructed counts in high density regions such as the spine, presumably due to the increased probability of scattering in that area. Thus, the presence of scatter in the projections causes a redistribution of counts from areas of low attenuation toward areas of high attenuation. This finding has also been reported in positron emission tomography using a scanner with interplane septa retracted (*32*). We have also noted this effect using statistical reconstruction methods where scatter was neglected, indicating that the artifacts are independent of the reconstruction algorithm used. These results further emphasize the need for scatter correction taking variable attenuation into account along with accurate attenuation correction, particularly in SPECT studies of the thorax.

The method described uses planar transmission measurements to modify the scatter estimate derived from planar projections of the object. Therefore, it only takes account of variable attenuation at the point of scattering and along the path toward the detector. It does not take account of the effect of variable attenuation on the initial transport of the photon prior to scattering. A more sophisticated implementation of the method might involve reconstructing the full three-dimensional volume of attenuation data and taking the initial photon path into account using, for example, Monte Carlo techniques. Such an implementation, however, would be computationally demanding and impractical for routine use. We are currently investigating a practical alternative to the current transmission-dependent method that uses nonstationary convolution based on reconstructed attenuation images to more accurately model photon transport, with only single scattering events being considered.

Transmission data form the basis for the quantitative SPECT method used in this department including the scatter correction method described in this report. The methodology for simultaneously acquiring emission and transmission data has been developed for single (*1,27,33*) and multiple detector gamma cameras (*34*). In this department, a collimated scanning line source is used which allows any combination of emission and transmission radionuclides with a maximum 10% increase in acquisition time (*27*). Therefore, it is no longer impractical to acquire transmission data on various SPECT instruments for quantitative corrections on a range of clinical studies. Implementation of the transmission-dependent method involves a straightforward modification to the more standard convolution-subtraction algorithm (*8*). When used in combination with a two-step measured attenuation correction, as in Method 4 of the phantom studies, processing takes less than 8 sec per slice using 64 × 64 matrices on a Sun SPARCstation 10/30 computer (86 Mips) (Sun Microsystems, Mountain View, CA), including flood correction, prefiltering, reconstruction and forward projection steps. Therefore, quantitative corrections using this scheme can be performed in a practical time.

The practical application of the quantitative method has been further enhanced by the extension of transmission-dependent scatter correction to ^{201}Tl studies with application in, for example, myocardial perfusion and tumor viability studies. There is no theoretical impediment to extending the method to other radionuclides. Since the modified buildup equation holds well for both ^{99m}Tc and ^{201}Tl and since two of the three parameters have been found to be independent of photon energy, the remaining parameter could be determined from a simplified buildup experiment with perhaps only two or three measurements.

CONCLUSION

Transmission-dependent scatter correction has been validated using line source measurements and accurately predicts the scatter distribution in a challenging geometry with variable attenuation. The qualitative effect of scatter on a

range of clinical imaging situations was investigated using a realistic thorax phantom. The presence of scatter in the measured projections results in enhanced counts in high density regions such as the heart and spine and accurate attenuation correction alone does not remove these artifacts. Transmission-dependent scatter correction removes the artifacts and quantitative accuracy was better than 95% in separate heart and lung experiments. By comparison, convolution-subtraction overestimates scatter in the lungs and underestimates scatter in the heart due to the use of a constant scatter fraction that is inappropriate for heterogeneous objects. Transmission-dependent scatter correction has been developed for use with ^{99m}Tc and ^{201}Tl sources and offers potential for extension to other radionuclides.

ACKNOWLEDGMENTS

This work was supported in part by the National Health and Medical Research Council (NHMRC) of Australia, research grant 920036. The scanning transmission line source was supplied by Nuclear Fields Pty Ltd., Sydney. The ^{153}Gd source was supplied by the department of nuclear medicine, St Vincent's Hospital, Sydney, and prepared by Australian Radioisotopes, a division of the Australian Nuclear Science and Technology Organization.

REFERENCES

1. Bailey DL, Hutton BF, Walker PJ. Improved SPECT using simultaneous emission and transmission tomography. *J Nucl Med* 1987;28:844–851.
2. Ljungberg M, Strand S-E. Attenuation correction in SPECT based on transmission studies and Monte Carlo simulations of build-up functions. *J Nucl Med* 1990;31:493–500.
3. Moore SC. Attenuation compensation. In: Ell P, Holman B, eds. *Computed emission tomography*. London: Oxford University Press; 1982:339–360.
4. Gullberg GT, Huesman RH, Malko JA, Pelc NJ, Budinger TF. An attenuated projector-backprojector for iterative SPECT reconstruction. *Phys Med Biol* 1985;30:799–816.
5. Malko JA, Van Heertum RL, Gullberg GT, Kowalsky WP. SPECT liver imaging using an iterative attenuation correction algorithm and an external flood source. *J Nucl Med* 1986;27:701–705.
6. Manglos SH, Jaszczak RJ, Floyd CE, Hahn LJ, Greer KL, Coleman RJ. Nonisotropic attenuation in SPECT: phantom tests of quantitative effects and compensation techniques. *J Nucl Med* 1987;28:1584–1591.
7. Tsui BM, Gullberg GT, Edgerton ER, et al. Correction of non-uniform attenuation in cardiac SPECT imaging. *J Nucl Med* 1989;30:497–507.
8. Axelsson B, Msaki P, Israelsson A. Subtraction of Compton-scattered photons in single-photon emission computerized tomography. *J Nucl Med* 1984;25:490–494.
9. Jaszczak RJ, Greer KL, Floyd CE, Harris CG, Coleman RE. Improved SPECT quantitation using compensation for scattered photons. *J Nucl Med* 1984;25:893–900.
10. Msaki P, Axelsson B, Dahl CM, Larsson SA. Generalized scatter correction method in SPECT using point scatter distribution functions. *J Nucl Med* 1987;28:1861–1869.
11. Koral KF, Wang X, Rogers WL, Clinthorne NH, Wang X. SPECT Compton-scattering correction by analysis of energy spectra. *J Nucl Med* 1988; 29:195–202.
12. Mukai T, Links JM, Douglass KH, Wagner Jr HN. Scatter correction in SPECT using non-uniform attenuation data. *Phys Med Biol* 1988;33:1129–1140.
13. Gagnon D, Todd-Pokropek A, Arsenault A, Dupras G. Introduction to holospectral imaging in nuclear medicine for scatter subtraction. *IEEE Trans Med Imag* 1989;8:245–250.
14. Ljungberg M, Strand S-E. Scatter and attenuation correction in SPECT using density maps and Monte Carlo simulated scatter functions. *J Nucl Med* 1990;31:1560–1567.
15. Ogawa K, Harata Y, Ichihara T, Kubo A, Hashimoto S. A practical method for position-dependent Compton-scatter correction in single photon emission CT. *IEEE Trans Med Imag* 1991;10:408–412.
16. King MA, Hademenos GJ, Glick SJ. A dual-photopeak window method for scatter correction. *J Nucl Med* 1992;33:605–612.
17. Meikle SR, Hutton BF, Bailey DL, Fulton RR, Schindhelm K. SPECT scatter correction in non-homogeneous media. In: Colchester ACF, Hawkes DJ, eds. *Information processing in medical imaging, 12th international conference*. Berlin: Springer-Verlag; 1991:34–44.
18. Yanch JC, Flower MA, Webb S. Improved quantification of radionuclide uptake using deconvolution and windowed subtraction techniques for scatter compensation in single photon emission computed tomography. *Med Phys* 1990;17:1011–1022.
19. Galt JR, Cullom SJ, Garcia EV. SPECT quantification: a simplified method of attenuation and scatter correction for cardiac imaging. *J Nucl Med* 1992;33:2232–2237.
20. Ljungberg M, Strand S-E. Attenuation and scatter correction in SPECT for sources in a nonhomogeneous object: a Monte Carlo study. *J Nucl Med* 1991;32:1278–1284.
21. Penney BC, Rajeevan N, Bushe HS, Hademenos G, King MA. A scatter reduction method for In-111 scintigrams using five energy windows. *IEEE medical imaging conference*. Santa Fe, NM: IEEE; 1991:1866–1873.
22. Bailey DL, Hutton BF, Meikle SR, Fulton RR, Jackson CB. Iterative scatter correction incorporating attenuation data. *Eur J Nucl Med* 1989;15: 542.
23. Hubbell JH. A power series buildup factor formulation. Application to rectangular and off-axis disk source problems. *J Res NBS* 1963;67C:291–306.
24. Wu RK, Siegal JA. Absolute quantitation of radioactivity using the buildup factor. *Med Phys* 1984;11:189–192.
25. Larsson SA. Gamma camera emission tomography. Development and properties of a multi-sectional emission computed tomography system. *Acta Radiol Suppl* 1980;363:17–32.
26. Hubbell JH. Photon cross sections, attenuation coefficients and energy absorption coefficients from 10 keV to 100 GeV. *National Bureau of Standards, U.S. Department of Commerce* 1969;NSRDS-NBS:29.
27. Tan P, Bailey DL, Meikle SR, Eberl S, Fulton RR, Hutton BF. A scanning line source for simultaneous emission and transmission measurements in SPECT. *J Nucl Med* 1993;34:1752–1760.
28. Chang LT. A method for attenuation correction in radionuclide computed tomography. *IEEE Trans Nucl Sci* 1978;NS-25:638–643.
29. Bailey DL, Meikle SR, Eberl S, Fulton RR, Hooper PK, Hutton BF. A quantitative SPECT regime. *Conference record of the 1992 IEEE medical imaging conference*. Orlando, FL: IEEE; 1992:1005–1007.
30. Axelsson B, Israelsson A, Larsson SA. Studies of a technique for attenuation correction in single photon emission computed tomography. *Phys Med Biol* 1987;32:737–749.
31. Morozumi T, Nakajima M, Ogawa K, Yuta S. Attenuation correction methods using the information of attenuation distribution for single photon emission CT. *Med Imag Technol* 1984;2:20–28.
32. Cherry SR, Meikle SR, Hoffman EJ. Correction and characterization of scattered events in three-dimensional PET using scanners with retractable septa. *J Nucl Med* 1993;34:671–678.
33. Frey EC, Tsui BMW, Perry JR. Simultaneous acquisition of emission and transmission data for improved thallium-201 cardiac SPECT imaging using a technetium-99m transmission source. *J Nucl Med* 1992;33:2238–2245.
34. Tung C-H, Gullberg GT, Zeng GL, Christian PE, Datz FL, Morgan HT. Non-uniform attenuation correction using simultaneous transmission and emission converging tomography. *IEEE Trans Nucl Sci* 1992;39:1134–1143.